2025 23rd European Control Conference (ECC)
June 24-27, 2025. Thessaloniki, Greece

Data-driven Performance Optimization for Direct Air Capture Process

Amirreza Silani[1], Mohammad Khosravi[2], and Tim M.J. Nijssen[3]

Abstract— **Achieving the Paris Agreement's goal necessitates not only reducing carbon dioxide emissions to net zero but also actively removing CO_2 from the atmosphere. Direct Air Capture (DAC) emerges as a pivotal technology in this effort, offering a reliable, flexible, and scalable solution for negative emissions. However, DAC performance is highly sensitive to environmental factors such as temperature and humidity. Consequently, it is vital to develop dynamic control and optimization mechanisms that can enhance the cost-efficiency of DAC. Due to the complexity and lack of a comprehensive model for DAC systems, the need for expert knowledge for modeling, and high computational costs, traditional model-based methods are not feasible. Therefore, we suggest a model-free, data-driven optimization technique based on Bayesian optimization to enhance the productivity and cost-effectiveness of DAC.**

I. INTRODUCTION

The Paris Agreement aims to limit global warming to 1.5 °C [1], but achieving this goal faces significant challenges. Limited supplies of crucial materials like cobalt and lithium hinder the transition to electric vehicles, allowing CO_2-emitting cars to persist. Similarly, the aviation sector continues to be a major source of emissions with few alternatives to fossil fuels. To address these issues, the *Carbon Dioxide Removal* (CDR) industry must scale up to remove CO_2 [2]–[4]. Direct Air Capture (DAC) is a leading CDR technology, using solid sorbents to extract CO_2 from the air, which is then stored or repurposed [5]. Despite its flexibility and potential for integration with renewable energy, DAC is highly energy-intensive [3], [6]. Furthermore, DAC performance is sensitive to environmental factors like temperature and humidity, which can raise costs by up to 100% under unfavorable conditions [7], [8]. Hence, optimizing DAC for cost-efficiency and operational effectiveness in real-world conditions is crucial for its large-scale adoption.

The current scientific research efforts towards DAC are primarily focused on sorbent and process development at steady-state laboratory conditions [9]–[12]. Integrating DAC with existing Heating, Ventilation, and Air Conditioning (HVAC) systems is suggested in [9] as a strategy to leverage existing infrastructure for decreasing energy consumption and improving efficiency. In [10], a comparative assessment of aqueous scrubbing and solid sorbent processes reveals that solid-sorbent-based systems perform better, with lower energy and exergy demands, and greater CO_2 productivity. A dynamic physics-based model for Temperature-Vacuum Swing Adsorption (TVSA) cycles is proposed in [11], demonstrating that environmental factors such as weather and humidity fluctuations significantly affect DAC performance. Moreover, variations in ambient temperature and humidity are introduced as critical influences on energy consumption and CO_2 productivity. A static optimization problem is developed in [12] and solved to enhance DAC performance. These studies highlight the importance of optimizing DAC systems for energy efficiency and adaptability to environmental conditions. However, these works are primarily focused on steady-state laboratory conditions and do not address dynamic optimization approaches.

A data-driven approach is particularly justified for DAC due to the challenges associated with model-based methods. Developing physics-based DAC models requires expert knowledge of thermodynamics, heat and mass transfer, and Computational Fluid Dynamics (CFD) [13]. While DAC systems generally adhere to these principles, the specifics of their design vary by different manufacturers. Moreover, many producer companies do not disclose the exact design and operational parameters of their systems, making accurate modeling difficult. Additionally, DAC models are often parametric, requiring parameter estimation, which is difficult to achieve without extensive data or full measurements. Even if a detailed model were available, tuning the model to match real-world performance would involve solving highly complex, nonconvex Partial Differential Equation (PDE) constrained optimization problems. These optimization problems are computationally demanding and not always practical for real-time operations. Given these constraints, in this paper, we propose a data-driven, model-free optimization approach that bypasses the need for detailed system models. Specifically, we use Bayesian optimization [14]–[16], a powerful method that efficiently explores the solution space and optimizes system performance [17]–[23].

II. PERFORMANCE OPTIMIZATION PROBLEM FOR DAC PROCESS

This section outlines the operation of a pilot-scale Direct Air Capture (DAC) unit that employs a Steam-assisted Temperature Vacuum Swing Adsorption (S-TVSA) process. DAC is a leading Carbon Dioxide Removal (CDR) technology, using solid sorbents to extract CO_2 from the air, and S-TVSA is the most commonly applied DAC method

[1]Amirreza Silani is with the Faculty of Mechanical Engineering, Department of Process and Energy and Delft Center for Systems and Control, Delft University of Technology, 2628 CB, Delft, The Netherlands and Wind Energy Group, TNO, 2288 GH, Rijswijk, The Netherlands a.silani@tudelft.nl, amirreza.silani@tno.nl

[2]Mohammad Khosravi is with the Faculty of Mechanical Engineering, Delft Center for Systems and Control, Delft University of Technology, 2628 CD, Delft, The Netherlands mohammad.khosravi@tudelft.nl

[3]Tim M.J. Nijssen is with the Faculty of Mechanical Engineering, Department of Process and Energy, Delft University of Technology, 2628 CB, Delft, The Netherlands t.m.j.nijssen@tudelft.nl

that combines temperature and vacuum swings with steam assistance to enhance CO_2 capture efficiency [5]. The S-TVSA process extracts CO_2 from ambient air through a series of stages: (1) adsorption, (2) evacuation, (3) heating, (4) desorption, (5) cooling, and (6) repressurization (see Fig. 1). During the adsorption phase, CO_2 molecules react chemically with amine functional groups located on the adsorbent's interior surfaces, adhering to them. When the adsorbent reaches its saturation point, the adsorption phase concludes. The following steps, stages (2) through (6), are collectively known as *regeneration*. This regeneration process serves to release the concentrated CO_2 from the sorbent while simultaneously preparing the adsorbent for the next cycle of CO_2 capture [11], [13]. The processes of adsorption and desorption are described by thermodynamics, heat and mass transfer laws, which are represented by Partial Differential Equations (PDEs) that introduce complexity into the modeling of these phenomena. Notably, the heating and cooling processes involved in regeneration are also governed by thermodynamic laws, further complicating the dynamics through the application of PDEs.

Developing detailed, physics-based models for DAC requires an advanced understanding of several complex fields, including thermodynamics, heat and mass transfer, and fluid dynamics. These models typically simulate the intricate physical processes involved in CO_2 capture, such as adsorption kinetics, pressure and temperature fluctuations, and air-sorbent interactions [24]–[27]. However, despite the DAC process following these general scientific principles, the specific design and operational nuances of each DAC system can vary widely depending on the manufacturer. As a result, creating a comprehensive, universally applicable model for DAC becomes extremely difficult, as the precise configuration directly influences performance metrics like energy efficiency, CO_2 capture rates, and regeneration costs. Beyond these proprietary barriers, DAC systems are inherently parametric in nature, meaning that their performance is governed by a wide range of variables such as the characteristics of the sorbent material. Therefore, accurate modeling requires precise estimation of these parameters, which in turn depends on large amounts of data that are often unavailable. Comprehensive datasets, including real-time operational measurements and environmental variables, would be needed to properly tune the model to reflect real-world operating conditions. However, such data is difficult to obtain in practice, particularly when DAC systems are operated in varying climate conditions. This lack of data makes it challenging to ensure that model-based approaches align with actual system. Even in cases where parameter estimation is feasible, the subsequent task of tuning these models to match actual DAC system behavior involves solving highly complex, nonconvex PDE constrained optimization problems. These optimization problems are computationally expensive to solve and can be even intractable. As a result, the model-based optimization methods are not well-suited for DAC systems.

Given these challenges for the model-based approaches,

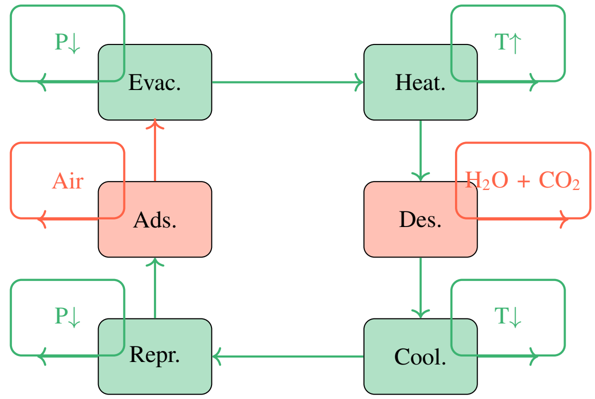

Fig. 1. The S-TVSA process steps with temperature and pressure indicators.

we propose a data-driven, model-free optimization approach that bypasses the need for detailed system models. Specifically, we employ Bayesian optimization, a powerful method that efficiently explores the solution space and optimizes system performance with minimal computational cost. The overall performance of the DAC process depends on key decision variables, including the adsorption, heating, desorption, and cooling times, the superficial gas velocity, the reference temperature of heat and cool sources, and the purge gas flow rate. Bayesian optimization can systematically identify optimal operating conditions that minimize the DAC costs and maximize its productivity. This approach leverages the data produced by a high fidelity model to adapt to variations in system behavior and varying climate conditions, allowing us to optimize the DAC process effectively. Furthermore, this framework is adaptable, i.e., one can substitute actual plant data as it becomes available, allowing for even more accurate and tailored optimization over time.

We consider the main decision variables, namely adsorption time (t_{ads}), heating time (t_{heat}), desorption time (t_{des}) and cooling time (t_{cool}), on which the overall performance of the DAC process depends. Moreover, the DAC process is highly sensitive to the ambient temperature T_{amb} and relative humidity RH_{amb}, which are considered as the system disturbances [7], [8]. Indeed, the ambient temperature appears in the initial condition of temperature during adsorption, while the relative humidity affects the reaction rate of components. Accordingly, we define the vector of decision variables ξ as

$$\xi := [t_{\text{ads}},\ t_{\text{heat}},\ t_{\text{des}},\ t_{\text{cool}}]^\top, \tag{1}$$

and the vector of disturbances δ as

$$\delta := [T_{\text{amb}}, RH_{\text{amb}}]^\top. \tag{2}$$

In order to improve the performance of the DAC process, it is required to minimize the energy costs and maximize the productivity of DAC process, i.e., we need to solve the optimization problem

$$\begin{aligned} &\min_{\xi\in\Xi}\ f(\xi,\delta) \\ &\text{s.t. DAC dynamics} \end{aligned} \tag{3}$$

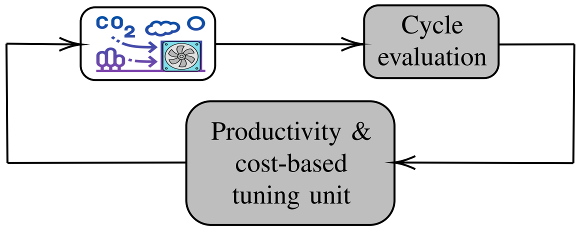

Fig. 2. Performance-based tuning scheme.

with the objective function f is defined as

$$f(\xi,\delta) = W_1 C_{\mathrm{T}}(\xi,\delta) - W_2 P_{\mathrm{T}}(\xi,\delta),$$

where

$$\begin{aligned} C_{\mathrm{T}}(\xi,\delta) = E_{\mathrm{r,CO_2}} + E_{\mathrm{r,H_2O}} + E_{\mathrm{sens,s}} \\ + E_{\mathrm{sens,r}} + E_{\mathrm{purge}} + E_{\mathrm{feed}} + E_{\mathrm{vac}} \end{aligned}$$

is the total cost of DAC process, $P_{\mathrm{T}}(\xi,\delta)$ is the productivity of DAC process, W_1, W_2 are the weight constants, and Ξ is the feasible set for ξ. Further details on costs and productivity are available in [13, Chapter 3].

III. Bayesian Optimization Approach

For a given $\xi \in \Xi$ and $\delta \in \Delta$, with the uncertainty set Δ, the value of the objective function $f(\xi,\delta)$, can be determined by conducting an experiment in which the decision variables are set to ξ. During the experiment, the system undergoes a full operational cycle, and the objective function is computed from the resulting complete cycle of the adsorption, evacuation, heating, desorption, and cooling steps. In order to lower the number of invoking this experimental *oracle*, Bayesian optimization (BO) is utilized [15]–[17], which is a powerful approach recognized for its utility in control process applications [28]. More precisely, BO is a method that leverages data to obtain optimal variables through a series of limited experiments. It relies on a surrogate model to approximate the cost function, guiding the optimization process efficiently [14]. To achieve this, Gaussian process regression [29] is employed to create a surrogate model for the objective function while also assessing the process uncertainties and disturbances. Fig. 2 shows the performance-based tuning scheme of Bayesian optimization method for the DAC process.

Let $\xi_{\mathrm{init}} := \{\xi \in \Xi \mid i = 1,\ldots,n_{\mathrm{init}}\}$ be an initial set of decision variables, which can be generated either by applying random feasible perturbations to its nominal values, or by using a Latin hypercube experimental design to create a maximally informative ξ_{init} [30]. Now, consider the data set $\mathcal{B}_n := \{(\xi_i, f_i(\xi_i,\delta_i)) \mid i = i,\ldots,n\}$, where n is the index of iteration and ξ_i is the decision variable for the experiment i. We construct a surrogate model for f, at iteration $n \geq n_{\mathrm{init}}$, using the data set $\mathcal{B}_n$ and Gaussian Process Regression (GPR). This surrogate model is denoted by $\hat{f}_n$. Indeed, we consider a Gaussian process prior for the function f, represented as $\mathcal{GP}(\mu,\kappa)$, where $\mu : \Xi \to \mathbb{R}$ and $\kappa : \Xi \times \Xi \to \mathbb{R}$ are the mean and kernel functions in the Gaussian process prior for f, respectively. Let the information matrices be defined as $\boldsymbol{\xi}_n := [\xi_1,\ldots,\xi_n]^\top$ and $\boldsymbol{f}_n := [f_1(\xi_1,\delta_1),\ldots,f_n(\xi_n,\delta_n)]^\top$. Then, for any $\xi \in \Xi$, we have

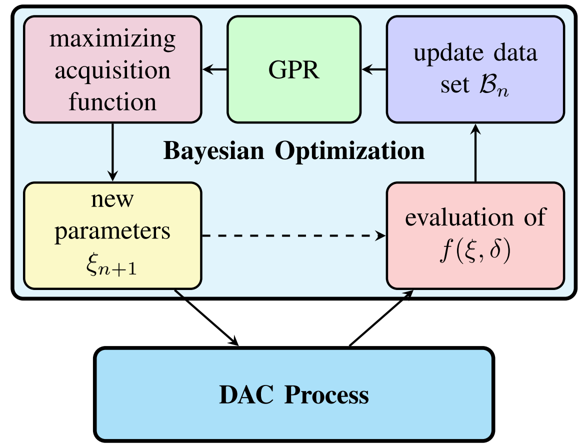

Fig. 3. Bayesian Optimization Process Diagram.

$$f(\xi) \sim \mathcal{N}(\mu_n(\xi), \omega_n(\xi)), \tag{4}$$

where

$$\mu_n(\xi) = \mu(\xi) + \mathbf{k}_n(\xi)^\top (K_n + \sigma^2 \mathbb{I})^{-1} (\boldsymbol{f}_n - \mu(\boldsymbol{\xi}_n)) \tag{5}$$
$$\omega_n(\xi) = \kappa(\xi,\xi) - \mathbf{k}_n(\xi)^\top (K_n + \sigma^2 \mathbb{I})^{-1} \mathbf{k}_n(\xi), \tag{6}$$

are the mean and variance, respectively, with the identity matrix $\mathbb{I}$ and the variance of uncertainty σ^2. Moreover, we define $\mathbf{k}_n(\xi) := [\kappa(\xi,\xi_1),\ldots,\kappa(\xi,\xi_n)]^\top \in \mathbb{R}^n$, $\mu(\boldsymbol{\xi}_n) := [\mu(\xi_1),\ldots,\mu(\xi_n)]^\top \in \mathbb{R}^n$, and $K_n := [\kappa(\xi_p,\xi_q)]_{p,q=1}^n \in \mathbb{R}^{n\times n}$.

By utilizing these probabilistic surrogate models for the function f, we are able to choose the parameters $\xi_{n+1} \in \Xi$ to be used in the next experiment and for future calculations of $f_i(\xi_i,\delta_i)$. To balance exploration and exploitation, we define the expected improvement function $E_n : \Xi \to \mathbb{R}$ as an acquisition function, which aims to select ξ that maximizes the expected improvement in performance and is given by

$$E_n(\xi) := (\chi_n(\xi)\Psi(\chi_n(\xi)) + \psi(\chi_n(\xi)))\,\omega_n(\xi)^{\frac{1}{2}}, \tag{7}$$

where $\chi_n(\xi) = (\mu_n(\xi) - f_n^+)/\omega_n(\xi)^{\frac{1}{2}}$, f_n^+ is the minimal cost associated with the first n experiments, Ψ is the cumulative distribution function and ϕ is the probability density function of the standard normal distribution.

Using *Particle Swarm Optimization (PSO)*, the following optimization is solved to obtain the next vector of decision variables:

$$\xi_{n+1} := \arg\max_{\xi\in\Xi} E_n(\xi). \tag{8}$$

When ξ_{n+1} is computed, a new experiment with the decision variable ξ_{n+1} is executed. Then, the data set $\mathcal{B}_{n+1} = \mathcal{B}_n \cup \{(\xi_{n+1}, f_{n+1}(\xi_{n+1},\delta_{n+1})))\}$ is updated. This procedure is repeated until convergence to the solution of (3) is achieved. Fig. 3 shows the process of Bayesian optimization approach.

IV. High-Fidelity Model Details for Numerical Validation of Data-Driven Approach

In this section, we introduce a model that acts as a high-fidelity model to validate our proposed data-driven approach. Specifically, we introduce the detailed model of Lewatit®VP OC 1065 as a ground truth model [11], [13], [31], [32]. The sorbent's properties, such as CO_2 adsorption capacity, reaction kinetics, and chemical stability, are described in [11], [24]–[27]. For ease of discussion, the parameters of the model are provided in Table I in the appendix.

The adsorption model is characterized by a series of time-dependent Partial Differential Equations (PDEs) [11], [13], [31], [32]. A key assumption in this model is that the gas velocity remains constant during adsorption, given the relatively low concentrations of the adsorbed species. Consequently, this leads to the establishment of mass balance equations for the gas phase concerning CO_2 and H_2O, *i.e.*, (9) and (10), as well as mass balance equations for the solid phase pertaining to CO_2 and H_2O, *i.e.*, (11) and (12), respectively. Additionally, the model includes a thermal energy balance equation, *i.e.*, (13).

$$\begin{aligned}\varepsilon_\mathrm{r}\partial_t c_{\mathrm{CO_2,g}} &= \partial_z\left(D_{\mathrm{ax,CO_2}}\partial_z c_{\mathrm{CO_2,g}} - u_\mathrm{g}c_{\mathrm{CO_2,g}}\right)\\ &\quad -(1-\varepsilon_\mathrm{r})\rho_\mathrm{s}\partial_t q_{\mathrm{CO_2}} \qquad (9)\\ \varepsilon_\mathrm{r}\partial_t c_{\mathrm{H_2O,g}} &= \partial_z\left(D_{\mathrm{ax,H_2O}}\partial_z c_{\mathrm{H_2O,g}} - u_\mathrm{g}c_{\mathrm{H_2O,g}}\right)\\ &\quad -(1-\varepsilon_\mathrm{r})\rho_\mathrm{s}\partial_t q_{\mathrm{H_2O}} \qquad (10)\\ \partial_t q_{\mathrm{CO_2}} &= R_{\mathrm{CO_2}}\eta_{\mathrm{CO_2}} \qquad (11)\\ \partial_t q_{\mathrm{H_2O}} &= R_{\mathrm{H_2O}}\eta_{\mathrm{H_2O}} \qquad (12)\\ \left(\left(1-\varepsilon_\mathrm{r}\right)\rho_\mathrm{s}C_{\mathrm{p,s}} + \varepsilon_\mathrm{r}\rho_\mathrm{g}C_{\mathrm{p,g}}\right)\partial_t T &=\\ \partial_z\left(\lambda_{\mathrm{s,eff}}\partial_z T - u_\mathrm{g}\rho_\mathrm{g}C_{\mathrm{p,g}}T\right)&\\ +(1-\varepsilon_\mathrm{r})\rho_\mathrm{s}\big(\Delta H_{\mathrm{r,CO_2}}\partial_t q_{\mathrm{CO_2}}&\\ +\Delta H_{\mathrm{r,H_2O}}\partial_t q_{\mathrm{H_2O}}\big) + Q_{\mathrm{source}}, &\qquad (13)\end{aligned}$$

where and $Q_{\mathrm{source}} = 0$ for adsorption, $R_{\mathrm{CO_2}}$, k_T, $q_{\mathrm{eq,CO_2}}$, t_h, b, q_s, $\eta_{\mathrm{CO_2}}$, ϕ_{th}, $R_{\mathrm{H_2O}}$, RH, $p^{\mathrm{sat}}_{\mathrm{H_2O}}$, $q_{\mathrm{eq,H_2O}}$, C_{GAB}, k_{GAB}, k_{LDF}, and $\eta_{\mathrm{H_2O}}$ are given in the appendix and [13, Chapter 3]. Moreover, Danckwerts boundary conditions are applied to the PDEs and the initial conditions set as the final conditions from the previous stage, which are given in [13, Chapter 3].

A unified heat transfer model is employed to address both the heating and cooling phases. This model concentrates specifically on the thermal behavior within the bed, thus only determining the variations in temperature as follows:

$$((1-\varepsilon_\mathrm{r})\rho_\mathrm{s}C_{\mathrm{p,s}} + \varepsilon_\mathrm{r}\rho_\mathrm{g}C_{\mathrm{p,g}})\partial_t T = \lambda_{\mathrm{s,eff}}\partial_z^2 T + Q_{\mathrm{source}}, \quad (14)$$

with $Q_{\mathrm{source}} = \delta(z)h_\mathrm{t}a_\mathrm{s}(T_{\mathrm{ht}} - T)$, where T_{ht} is the temperature of heat or cool sources and the function $\delta(z)$ is characterized as a Dirac-delta function, which takes a value of one at the positions of heat sources and zero elsewhere. Further details on the boundary and initial conditions are given in [13, Chapter 3]. Additionally, we use the ideal gas law to model the evacuation and repressurization stages.

The desorption model operates on the same foundational principles as the adsorption model concerning mass and energy transport. Hence, The dynamic model for desorption is the same as (9)-(13), with Danckwerts boundary conditions, the initial conditions which are set as the final conditions from the previous stage, and $\eta_{\mathrm{CO_2}} = 1$ (see [13, Chapter 3] for further details). However, the assumption of a constant gas velocity does not hold, particularly during desorption at lower absolute pressures. Instead, we assume the desorption pressure to be kept constant by the vacuum pump, calculating the gas velocity from the amount of desorbing gas. Thus, to obtain the changing gas velocity, we consider

$$\varepsilon_\mathrm{r}\frac{p}{RT^2}\partial_t T = \frac{p}{R}\partial_z\left(\frac{u_\mathrm{g}}{T}\right) + (1-\varepsilon_\mathrm{r})\rho_\mathrm{s}\sum_{i=1}^{n}\partial_t q_i. \quad (15)$$

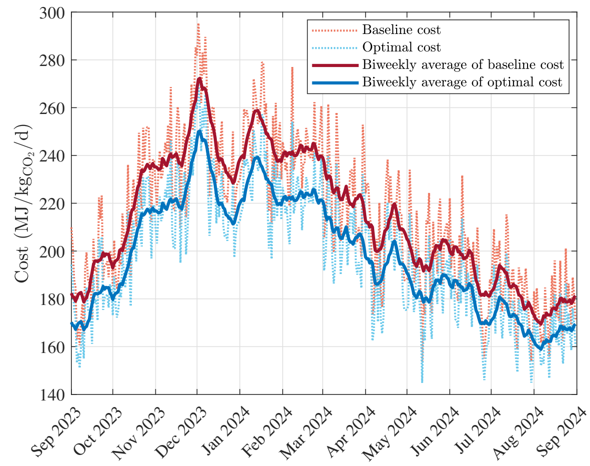

Fig. 4. DAC cost: the comparison between the proposed and baseline approach.

The energy needs for the S-TVSA process are categorized into seven distinct components: the energy required for the CO_2 endothermic desorption ($E_{\mathrm{r,CO_2}}$), energy required for the H_2O desorption ($E_{\mathrm{r,H_2O}}$), sorbent sensible heat ($E_{\mathrm{sens,s}}$), reactor sensible heat ($E_{\mathrm{sens,r}}$), latent and sensible heat of the purge gas (E_{purge}), feed compression energy (E_{feed}), and vacuum compression energy (E_{vac}). Moreover, we consider the productivity (P_T) for the process. Further details on costs and productivity are available in [13, Chapter 3].

V. Numerical Experiments

In this section, the performance of the proposed data-driven approach is verified in simulation. We used the DAC process model described in Section IV [11], [13], [31], [32] as our high-fidelity model for performing the experiments. The parameters of the model are described in Table I in the appendix. To solve PDEs (9)-(15), the domain is discretized spatially, then the resulting system of discretized differential equations is solved in MATLAB using its ODE solver. We used temperature and relative humidity data from September 1, 2023, to September 1, 2024, from the weather station at Schiphol Airport in Amsterdam [33] as the disturbance. Subsequently, we employ the Bayesian optimization approach outlined in Section III to solve the optimization problem (3). Specifically, our objective is to simultaneously minimize

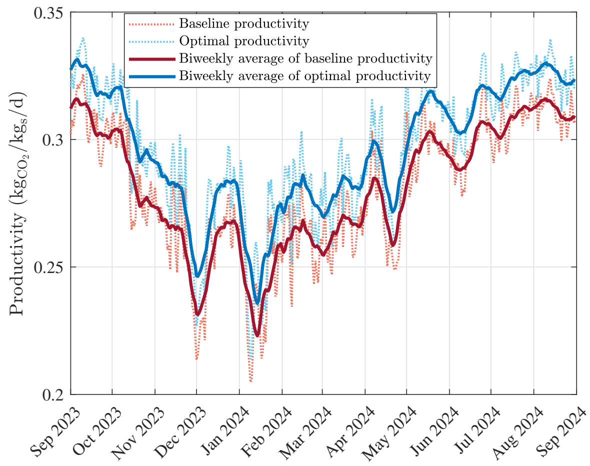

Fig. 5. DAC productivity: the comparison between the proposed and baseline approach.

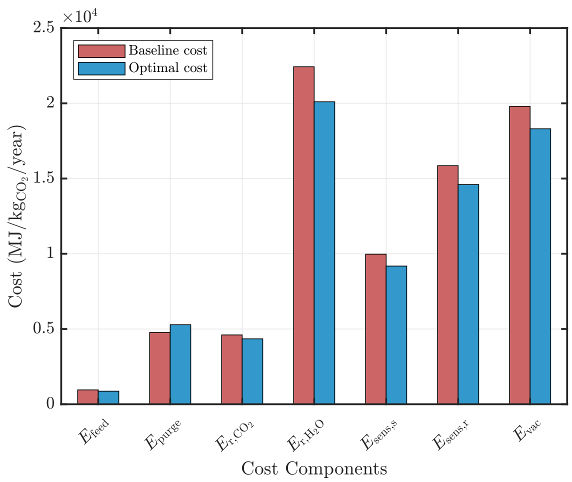

Fig. 6. DAC cost components: the comparison between the proposed and baseline approach.

the costs and maximize the productivity of DAC processes. For benchmarking purposes, we compare our results against the performance of methods previously proposed in [13], using them as a baseline to highlight the advantages of our approach. We can observe from Fig. 4 that the proposed Bayesian optimization method achieves a substantial reduction in daily DAC capture costs, achieving a 7.26% decrease relative to the baseline method. This cost reduction underscores the efficiency of our approach in enhancing the economic feasibility of DAC technologies, particularly when operational cost minimization is a priority. Additionally, Fig. 5 demonstrates an improvement in DAC productivity, with a 5.45% increase over the baseline method. This productivity gain highlights the capability of the Bayesian optimization framework to identify configurations that not only reduce expenses but also improve operational performance, thereby contributing to the scalability and practicality of DAC in real-world applications. Finally, Fig. 6 demonstrates a detailed comparison of DAC cost components under both our proposed approach and the baseline method. We can notice that the highest cost component is associated with the energy consumption for the desorption of H_2O, while the lowest cost component is the compression energy for the feeding fan. Thus, the cost-effectiveness and productivity enhancements achieved by our proposed data-driven approach emphasize its potential to make DAC financially feasible.

VI. Conclusions and Future Work

Direct Air Capture (DAC) plays a crucial role in meeting the Paris Agreement's goal by offering a scalable and flexible solution for negative emissions. However, the sensitivity of DAC to environmental conditions necessitates the development of advanced control and optimization strategies to improve cost-efficiency. Traditional model-based methods are not feasible due to the complexity and lack of a comprehensive model for DAC systems, the need for expert knowledge for modeling, and high computational costs. Thus, we proposed a data-driven, model-free approach based on Bayesian optimization. This technique provides an effective framework for enhancing DAC performance. Future works include developing model predictive control for DAC.

Acknowledgment

We would like to thank Dr. Maryam Khosroshahi for her valuable discussions on Bayesian optimization methods.

References

[1] United Nations, "The Paris Agreement," pp. 1–25, 2015.
[2] IPCC Working Group III, "Sixth assessment report, mitigation of climate change (technical summary)," 2021.
[3] National Academies of Sciences, Engineering and Medicine, *NETs and Reliable Sequestration*. National Academies Press, 3 2019.
[4] R. Höglund and K. Niparko, "Cdr.fyi," www.cdr.fyi.
[5] B. Kampman and K. Kruit et. al, "Koolstofverwijdering voor klimaatbeleid," CE Delft, Tech. Rep. 202209093, June 2023.
[6] Climeworks GA, "Orca: the first large-scale plant," climeworks.com/roadmap/orca, 2022. [Online]. Available: climeworks.com/roadmap/orca
[7] J. F. Wiegner and A. Grimm et al., "Optimal Design and Operation of Solid Sorbent DAC Processes at Varying Ambient Conditions," *Ind. Eng. Chem. Res.*, vol. 61, no. 34, pp. 12 649–12 667, 2022.
[8] C. J. E. Bajamundi and J. Koponen et al., "Capturing CO_2 from air: Technical performance and process control improvement," *J. CO_2 Util.*, vol. 30, no. 12, pp. 232–239, 2019.
[9] A. Sodiq, Y. Abdullatif, B. Aissa, A. Ostovar, N. Nassar, M. El-Naas, and A. Amhamed, "A review on progress made in direct air capture of CO_2," *Environmental Technology & Innovation*, vol. 29, p. 102991, 2023.
[10] F. Sabatino, A. Grimm, F. Gallucci, M. van Sint Annaland, G. J. Kramer, and M. Gazzani, "A comparative energy and costs assessment and optimization for direct air capture technologies," *Joule*, vol. 5, no. 8, pp. 2047–2076, 2021.
[11] H. Schellevis, T. Van Schagen, and D. Brilman, "Process optimization of a fixed bed reactor system for direct air capture," *International journal of greenhouse gas control*, vol. 110, p. 103431, 2021.
[12] J. F. Wiegner, A. Grimm, L. Weimann, and M. Gazzani, "Optimal design and operation of solid sorbent direct air capture processes at varying ambient conditions," *Industrial & Engineering Chemistry Research*, vol. 61, no. 34, pp. 12 649–12 667, 2022.
[13] M. Schellevis, "CO_2 capture from air: A process engineering approach," 2023.
[14] R. Garnett, *Bayesian optimization*. Cambridge University Press, 2023.
[15] B. Shahriari, K. Swersky, Z. Wang, R. P. Adams, and N. De Freitas, "Taking the human out of the loop: A review of bayesian optimization," *Proceedings of the IEEE*, vol. 104, no. 1, pp. 148–175, 2015.

TABLE I

DESCRIPTION OF SYMBOLS AND PARAMETERS (FOR PAIR VALUES, THE FIRST IS FOR CARBON DIOXIDE AND THE SECOND FOR WATER).

ΔH_0	Tóth heat of adsorption ($\mathrm{J\ mol^{-1}}$)	95.3×10^3
$\Delta_{\mathrm{c}} H$	difference in enthalpy between monolayer and multilayer ($\mathrm{J\ mol^{-1}}$)	-8.69×10^3
$\Delta_{\mathrm{k}} H$	difference in enthalpy between bulk liquid and multilayer ($\mathrm{J\ mol^{-1}}$)	-8.2×10^3
$\Delta_{\mathrm{r}} H_i$	reaction heat of component i ($\mathrm{J\ mol^{-1}}$)	75×10^3, 43×10^3
a_{s}	specific surface area ($\mathrm{m^2\ m_r^{-3}}$)	150
b	Tóth affinity constant ($\mathrm{Pa^{-1}}$)	(-)
b_0	Tóth affinity constant at reference temperature ($\mathrm{Pa^{-1}}$)	93×10^{-5}
C_0	Arrhenius pre-exponential factor for C_{GAB} (-)	100
C_{GAB}	Guggenheim constant in GAB isotherm (-)	(-)
C_{m}	monolayer capacity in GAB isotherm ($\mathrm{mol\ kg^{-1}}$)	5.55
$C_{\mathrm{p,g}}$	gas specific heat capacity ($\mathrm{J\ kg^{-1}\ K^{-1}}$)	1005
$C_{\mathrm{p,s}}$	solid specific heat capacity ($\mathrm{J\ kg^{-1}\ K^{-1}}$)	1580
c	concentration ($\mathrm{mol\ m^{-3}}$)	equations (9), (10)
D_{ax}	axial dispersion coefficient ($\mathrm{m^2\ s^{-1}}$)	(-)
E_{act}	activation energy ($\mathrm{J\ mol^{-1}}$)	15.2×10^3
h_{t}	heat transfer coefficient ($\mathrm{W\ m^{-2}\ K^{-1}}$)	150
u	superficial gas velocity ($\mathrm{m_g^3\ m_r^{-2}\ s^{-1}}$)	0.11
α	temperature dependency of t_{h} (-)	0.33
ε_{p}	void fraction of sorbent ($\mathrm{m_g^3\ m_r^{-3}}$)	0.23
ε_{r}	void fraction of reactor ($\mathrm{m_g^3\ m_r^{-3}}$)	0.4
$\lambda_{\mathrm{s,eff}}$	axial thermal conductivity ($\mathrm{W\ m^{-1}\ K^{-1}}$)	0.121
χ	temperature dependency of q_{s}	0
k_{GAB}	multilayer correction factor in GAB isotherm (-)	(-)
$k_{0,\mathrm{GAB}}$	Arrhenius pre-exponential factor for K_{GAB} (-)	0.92
k_0	Arrhenius pre-exponential factor for reaction rate ($\mathrm{mol\ kg^{-1}\ bar^{-1}\ s^{-1}}$, $\mathrm{s^{-1}}$)	3.5×10^{-2}, 450
k_{LDF}	linear driving force reaction rate constant ($\mathrm{s^{-1}}$)	(-)
k_{T}	Tóth reaction rate constant ($\mathrm{mol\ kg^{-1}\ bar^{-1}\ s^{-1}}$)	(-)
p	pressure (Pa)	(-)
q	sorbent loading ($\mathrm{mol\ kg^{-1}}$)	equations (11), (12)
q_{s}	Tóth maximum capacity ($\mathrm{mol\ kg^{-1}}$)	(-)
$q_{\mathrm{s},0}$	Tóth maximum capacity at reference temperature ($\mathrm{mol\ kg^{-1}}$)	3.40
R	ideal gas constant ($\mathrm{J\ mol^{-1}\ K^{-1}}$)	8.31446
R_i	reaction rate of component i ($\mathrm{mol\ kg^{-1}\ s^{-1}}$)	(-)
T	temperature (K)	equation (13)
T_0	Tóth reference temperature (K)	353.15
t_{h}	Tóth heterogeneity constant (-)	(-)
$t_{\mathrm{h},0}$	Tóth heterogeneity constant at T_0 (-)	0.37
z	axial direction (m)	(-)
δ	identification of energy point source in 1D model (-)	binary
η	effectiveness factor (-)	[0,1]
ρ	density ($\mathrm{kg\ m^{-3}}$)	1.204
Φ	gas flow rate ($\mathrm{g_{purge}\ min^{-1}}$)	1.04
g	gas phase	
i	components (CO_2 and H_2O)	
r	reactor	
s	solid phase	

[16] J. R. Gardner, M. J. Kusner, Z. E. Xu, K. Q. Weinberger, and J. P. Cunningham, "Bayesian optimization with inequality constraints." in *ICML*, vol. 2014, 2014, pp. 937–945.

[17] A. Rupenyan, M. Khosravi, and J. Lygeros, "Performance-based trajectory optimization for path following control using Bayesian optimization," in *2021 60th IEEE Conference on Decision and Control (CDC)*. IEEE, 2021, pp. 2116–2121.

[18] M. Nobar, J. Keller, A. Rupenyan, M. Khosravi, and J. Lygeros, "Guided Bayesian optimization: Data-efficient controller tuning with digital twin," *IEEE Transactions on Automation Science and Engineering*, 2024.

[19] M. Khosravi, A. Eichler, N. Schmid, R. S. Smith, and P. Heer, "Controller tuning by Bayesian optimization an application to a heat pump," in *2019 18th European Control Conference (ECC)*. IEEE, 2019, pp. 1467–1472.

[20] M. Khosravi, V. Behrunani, R. S. Smith, A. Rupenyan, and J. Lygeros, "Cascade control: Data-driven tuning approach based on Bayesian optimization," *IFAC-PapersOnLine*, vol. 53, no. 2, pp. 382–387, 2020.

[21] M. Khosravi, V. N. Behrunani, P. Myszkorowski, R. S. Smith, A. Rupenyan, and J. Lygeros, "Performance-driven cascade controller tuning with Bayesian optimization," *IEEE Transactions on Industrial Electronics*, vol. 69, no. 1, pp. 1032–1042, 2021.

[22] M. Khosravi, C. Konig, M. Maier, R. S. Smith, J. Lygeros, and A. Rupenyan, "Safety-aware cascade controller tuning using constrained Bayesian optimization," *IEEE Transactions on Industrial Electronics*, vol. 70, no. 2, pp. 2128–2138, 2023.

[23] M. Khosravi, N. Schmid, A. Eichler, P. Heer, and R. S. Smith, "Machine learning-based modeling and controller tuning of a heat pump," in *Journal of Physics: Conference Series*, vol. 1343, no. 1. IOP Publishing, 2019, p. 012065.

[24] W. R. Alesi Jr and J. R. Kitchin, "Evaluation of a primary amine-functionalized ion-exchange resin for CO_2 capture," *Industrial & engineering chemistry research*, vol. 51, no. 19, pp. 6907–6915, 2012.

[25] M. J. Bos, T. Kreuger, S. Kersten, and D. Brilman, "Study on transport phenomena and intrinsic kinetics for CO_2 adsorption in solid amine sorbent," *Chemical Engineering Journal*, vol. 377, p. 120374, 2019.

[26] A. Sayari, A. Heydari-Gorji, and Y. Yang, "CO_2-induced degradation of amine-containing adsorbents: reaction products and pathways," *Journal of the American Chemical Society*, vol. 134, no. 33, pp. 13 834–13 842, 2012.

[27] Q. Yu, J. d. l. P. Delgado, R. Veneman, and D. W. Brilman, "Stability of a benzyl amine based CO_2 capture adsorbent in view of regeneration strategies," *Industrial & engineering chemistry research*, vol. 56, no. 12, pp. 3259–3269, 2017.

[28] J. Tang, X. Lin, F. Zhao, and X. Chen, "Process quality control through bayesian optimization with adaptive local convergence," *Chemical Engineering Science*, vol. 293, p. 120039, 2024.

[29] M. Seeger, "Gaussian processes for machine learning," *International journal of neural systems*, vol. 14, no. 02, pp. 69–106, 2004.

[30] M. D. McKay, R. J. Beckman, and W. J. Conover, "A comparison of three methods for selecting values of input variables in the analysis of output from a computer code," *Technometrics*, vol. 42, no. 1, pp. 55–61, 2000.

[31] M. Schellevis, T. Jacobs, and W. Brilman, "CO_2 capture from air in a radial flow contactor: batch or continuous operation?" *Frontiers in Chemical Engineering*, vol. 2, p. 596555, 2020.

[32] Q. Yu and W. Brilman, "A radial flow contactor for ambient air CO_2 capture," *Applied Sciences*, vol. 10, no. 3, p. 1080, 2020.

[33] KNMI. (2024) Weerstations - dagwaarnemingen. 01-09-2024. [Online]. Available: https://daggegevens.knmi.nl/klimatologie/daggegevens